Mon. Not. R. Astron. Soc. **342,** 1349–1360 (2003)

A photometric–spectroscopic analysis and the evolutionary status of the Algol-type binary U Coronae Borealis

S. K. Yerli,[1,2⋆] M. J. Sarna,[3,1,2] S. Zola,[4,5] Robert Connon Smith[1] and G. Tovmassian[6]

[1]*Astronomy Centre, University of Sussex, Falmer, Brighton BN1 9QJ*
[2]*Middle East Technical University, Physics Department, 06531 Ankara, Turkey*
[3]*N. Copernicus Astronomical Centre, Polish Academy of Sciences, ul. Bartycka 18, 00–716 Warsaw, Poland*
[4]*Astronomical Observatory, Jagiellonian University, ul. Orla 171, 30–244 Cracow, Poland*
[5]*Mt. Suhora Observatory, Pedagogical University, ul. Podchorazych 2, 30-084 Cracow, Poland*
[6]*Observatorio Astronomico Nacional, IA UNAM, Aptdo Postal 877, 22800 Ensenada, BC, Mexico*

Accepted 2003 March 18. Received 2003 March 17; in original form 2002 June 13

ABSTRACT

The prime purposes of this study are to obtain reliable orbital parameters for the Algol-type binary U Coronae Borealis (U CrB) and to explain the evolutionary status of this system. All observations of the primary star's radial velocity are consistent with the value $K_1 = 58.6 \pm 2.0\,\mathrm{km\,s^{-1}}$. Measurements of the radial velocity of the secondary component give $K_2 = 185.2 \pm 5.0\,\mathrm{km\,s^{-1}}$. Using the photometrically determined inclination of 78.7 ± 0.3, the masses of the two stars are therefore deduced to be 4.74 ± 0.28 and $1.46 \pm 0.06\,\mathrm{M_\odot}$ for the primary and secondary components, respectively. Using all available observations, we discuss the origin and evolution of the close binary system U CrB. We derive the restrictions concerning masses and period from a general network of calculations of medium mass close binary evolution. Detailed models are calculated within the derived ranges, giving the most likely initial system parameters as $4.5\,\mathrm{M_\odot} + 2.7\,\mathrm{M_\odot}$ and $P_i = 1.4$ d. It turns out that the interactive evolution up to the present stage has been non-conservative. During its evolution, U CrB has lost about 14 per cent of its initial total mass ($\Delta M \sim 1\,\mathrm{M_\odot}$) and around 18 per cent of its initial total angular momentum. We also examine the possibility of probing dynamo action in the mass-losing component of U CrB. We point out that, in order to maintain the evolution of U CrB in its later stages, which is presumably driven by stellar 'magnetic braking', an efficient mechanism for producing large-scale surface magnetic fields in the donor star is required. We suggest that observed X-ray activity in U CrB may be a good indicator of its evolutionary status and the internal structure of the mass-losing component.

Key words: stars: abundances – binaries: eclipsing – binaries: spectroscopic – stars: evolution – stars: individual: U Coronae Borealis.

1 INTRODUCTION

The eclipsing binary U Coronae Borealis (U CrB) – see Table 1 – is one of the brightest Algol-type binaries. The larger but less massive secondary has filled its Roche lobe and is now transferring material to its companion. The primary component – the brighter member of the system (B6 V) – is partially eclipsed every 3.452 d. The secondary spectrum, which is seen during the partial eclipse, is F8 III–IV (Batten & Tomkin 1981).

In this paper we consistently denote the initially more massive star (the loser = mass-losing star, MLS) as the secondary, and the initially less massive star (the gainer = mass-accreting star, MAS) as the primary. For the observed semidetached systems, this is in agreement with the observers' tradition.

U CrB is an intensively studied object both in photometry as well as in spectroscopy (see Table 2). Photoelectric light curves (mostly in Johnson *UBV*) have been published by Kordylewski & Szafraniec (1957), Wood (1958), Catalano, Cristaldi & Lacona (1966) and Svolopoulos & Kapranidis (1972). Ultraviolet (UV) photometry (150–330 nm passbands) presented by Kondo, McCluskey & Wu (1981) does not show any modulation correlating with the orbital phase. In order to obtain more precise estimates of the absolute dimensions, the system was observed from 1980 to 1987 by van Gent (1989b) in four narrow passbands ($\Delta\lambda \sim 10$ nm) of the Utrecht

⋆E-mail: yerli@metu.edu.tr

Table 1. The basic data for U CrB. The epoch is the time of mid-eclipse.

Names	BD +32° 2569, HD 136175, SAO 64619
Comparison	BD +31° 2724, HD 137147 (var.) (Olson 1980)
	HD 136654 (van Gent 1989b)
α	$15^h18^m11\overset{s}{.}3$ (HMS) J2000.0
δ	$31°38'48\overset{''}{.}7$ (DMS) J2000.0
m_v	7.82
Eclipse	partial
$B-V$	+0.15 (MAS), −0.07 (MLS) (Wood 1958)
Sp.Type	B6 V + F8 III–IV (Batten & Tomkin 1981)
Epoch	2 440 367.8941 + 3.452 242 7E
	(Kreiner, private communication)

Photometric System (UPS; Heintze & van Gent 1989) ranging from 474 to 871 nm.

Previous spectroscopic work on U CrB was carried out by Batten & Tomkin (1981). Their work contains a collection of old spectroscopic data for both the primary – 138 spectrograms, 1919–1978, including spectra from Plaskett (1920) and Pearce (1935), one-prism spectrograph observations – and the secondary star (16 Reticon observations, 1979–1980). The section of their paper designated by *Other Lines* is the main data section, which contains velocities from the lines Ca II(K) 3933.664, Si II 4128.051, 4130.876, C II 4267.167, and Mg II 4481.228 Å. We found a typographic error in the *Miscellaneous Data* section (table 4 of Batten & Tomkin 1981). The point JD = 244 0427.765, $\phi = 0.54$ is well displaced from its real position in (figure 2 of the paper if the HJD of the given data is used. If the scattered data (especially from 1964–1967, modern prism spectrograms in Batten & Tomkin 1981) is avoided by excluding the outliers using the Powell method mentioned in Section 2.3, our results agree very well with theirs, except for the K_2 value (see Section 4 and Fig. 4).

A preliminary discussion of the evolutionary status of U CrB has been presented by Sarna (1992) and Sarna & de Greve (1996). They concluded that U CrB is a product of processes of either case A or more likely AB mass transfer with the initial mass ratio near 0.6, in which mass loss from the system was not negligible. They also suggested that, in the discussion of the evolutionary status, C and N abundances at the photosphere would be very useful.

In this paper we estimate orbital and physical parameters for U CrB, using all available photometric and spectroscopic data. In Section 2 we report on our spectroscopic observations and data reduction technique. In Section 3, we present details of the semi-amplitude measurement of the radial velocity (RV) curve. In Section 4 we show a synthetic light-curve solution for existing observational light and RV data using the Wilson–Devinney (WD) method (Wilson & Devinney 1971, revision 1992; Wilson 1992). A possible evolutionary status is calculated and presented in Section 6. In Section 7 we investigate the plausibility of dynamo operation in the mass-losing component of U CrB, and in Section 8 we give the conclusion.

2 OBSERVATIONS AND DATA REDUCTIONS

The ephemeris taken from Kreiner (private communication)

$$\text{HJD} = 2440367.8941 + 3.4522427E$$
$$\pm 0.0035 \qquad \pm 0.0000023$$

was used to determine the orbital phase at mid-exposure of each spectrum.

2.1 1994 data

We obtained 50 spectra of U CrB on the nights of 1994 March 17–24 using the Richardson–Brealey Spectrograph (RBS) at the 1-m Jacobus Kapteyn Telescope (JKT) at the Roque de los Muchachos Observatory on the island of La Palma. We used the 1200 grating with the EEV7 CCD which covers a wavelength range of 3725–4775 Å at a resolution of about 1.7 Å. The exposures were all 1000 s long. Almost a complete orbital cycle was covered during our observing run. A copper–argon arc spectrum was taken after three successive U CrB spectra to calibrate the wavelength and to correct for instrumental flexure and stability. The third-order polynomial fit to the positions of six unblended lines gave $\approx 10^{-3}$ Å discrepancy in the wavelength scale. Spectra of the spectrophotometric standard SP 1550+330 (=BD + 33 2642) (Oke & Gunn 1983) were also taken in order to correct for instrumental wavelength response.

After bias subtraction and dividing by the flat-field to correct for medium-scale sensitivity variations of the detector, optimal extraction (Horne 1986), as implemented by the FIGARO software package, was used to reduce the two-dimensional (2D) images to one-dimensional (1D) spectra. The arc spectra were extracted from the same region of the detector. These were used to obtain the wavelength scale for each object spectrum by interpolating from the wavelength scales of the two nearest spectra. Finally, to correct for the variations of instrumental response with wavelength and large-scale sensitivity variations, a calibration spectrum was created from the spectrophotometric standard using FIGARO tables of standards

Table 2. The list of important observations for U CrB (sorted by date).

Type	Filters and wavelengths (Å)	Reference
Johnson	V	Kordylewski & Szafraniec (1957)
Johnson	BV	Wood (1958)
Johnson	B	Bakos & Tremko (1981)
UV	1550, 1800, 2200, 2500, 3300	Kondo et al. (1981)
Spectroscopy	Ca II 3933, Si II 4128, 4130, C II 4267, Mg II	Batten & Tomkin (1981)
Strömgren	*uvby*	Olson (1982)
Spectroscopy	He I 4387, 4471, Mg II 4481, Fe II 4549	Olson (1984)
Narrow band	4740, 6720, 7810, 8710	van Gent (1989b), (UPS[a])
O I	7774	Etzel, Olson & Senay (1995)
H_α		Richards, Albright & Bowles (1995)
		Albright & Richards (1996)

Note: [a]Utrecht Photometric System (Heintze & van Gent 1989).

and procedures. The target spectra were then multiplied by this calibration spectrum, creating flux-corrected spectra.

2.2 1997 data

We obtained 42 Echelle spectra (grating with 79 lines mm^{-1} and 63° blaze angle) of U CrB on the nights of 1997 May 13–16, using ESPRESSO (Echelle Spectrograph for SPM) at the 2.1-m telescope of the Observatorio Astronómico Nacional (OAN) de San Pedro Mártir (SPM), Mexico. The slit length was kept fixed at 1.0 mm (=13.3 arcsec) by using appropriate masks on top of the main slit of length 30 mm. The cross-disperser angle was set to 353° which gave the orders 33–60 and the corresponding wavelength range of 6643–3793 Å. A 1024 × 1024 pixel CCD–TEK (24 μm pixel size) was used for recording. The spectrophotometric standard was 58 Aql (Hamuy et al. 1992).

After bias subtraction and flat-fielding, the extraction routine of IRAF – which is an adaptation of the optimal extraction routine designed by Horne (1986) – was used to reduce the 2D Echelle images to 1D spectra. The extraction was performed using trace information of the orders obtained while preparing the master flat-field. Using SPM's Th–Ar line list, more than 500 lines were identified. The final line list was reduced to 393 lines to decrease the positional error and to increase the interorder harmonization. The final positional rms error for all the arc frames was 0.0057 Å.

2.3 Radial velocity measurements

Radial velocities were calculated by cross-correlation using the IRAF Radial Velocity package, FXCOR; the peaks of the cross-correlation functions (CCFs) were measured by fitting Gaussian profiles. The template spectra for the primary were HD 43153 (B7V) and HD 155763 (B6III) for the 1994 and 1997 data, respectively. The template spectrum for the secondary for the 1997 data was HD 187691 (F8V).

After constructing the RV table, a robust optimization method (minimized absolute deviation), the POWELL routine of the software package (IDL 1997), was used to fit a sine curve to the data

$$\mathrm{RV}(\phi)_i = V_0 + K_i \sin\left(\frac{\phi - \phi_e}{p}\right) \quad (1)$$

where subscript i denotes the component (MAS or MLS), K_i is the amplitude of the RV curve, V_0 is the systemic velocity, ϕ is the epoch of the observation, ϕ_e is the epoch of the mid-eclipse, and p is the orbital period in days. A circular orbit was assumed in fitting. Free parameters in the fit were K_i and V_0.

This method turned out to be less sensitive to the details of the method (e.g. templates, weighting, etc.) than least-squares fitting and it gives reasonable fits even though the data contain outliers. However, we have to be careful if the data are concentrated at certain phase points with outliers. This distorts the optimization and pulls down (or pushes up) the curve while trying to 'optimize' the concentrated deviations. Therefore, in the case of abnormal fits, unwanted data had to be deleted from the input before the method was applied.

2.4 Stacked grey-scale spectra

Fig. 1 is divided into vertical sections, each containing a selected line region. At the top of each section, the corresponding line and its wavelength value are printed. The name and spectral type of the object and the RV template are printed at the top of the graph.

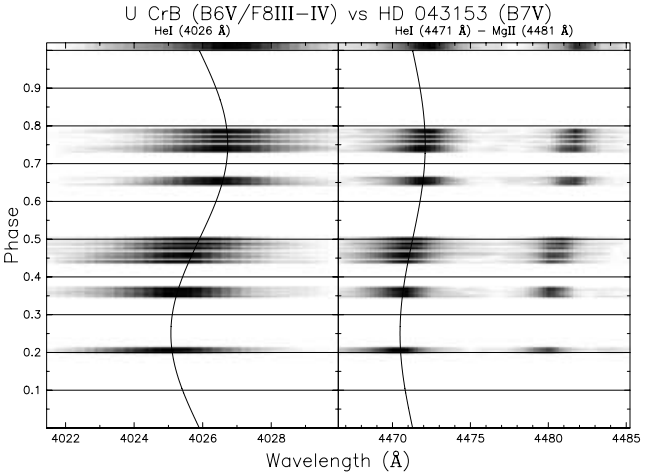

Figure 1. SGSS of U CrB for 1994 run (see Section 2.4 for details).

Underneath this information header lies a strip of the RV template's spectrum of the same line region. The vertical axis is divided into 1000 equal phase intervals. No clashes were found on the phase axis (i.e. each phase point is resolved for each observation). For eye comfort each phase point is copied one pixel above and below. For the chosen lines, the RV curve plot is overlaid on the corresponding line region. The rest wavelength of the line is used for this plot and corrected for V_0 of the cross-correlated RV standard.

3 RADIAL VELOCITY RESULTS

The cross-correlation was carried out only on selected lines, sampled with enough continuum around them. Even though the whole range of the spectrum (except the Balmer lines, etc.) is normally included in applying the cross-correlation technique (Hill 1993), disobeying that convention in this work had minor effects on the quality of results obtained. We had sufficient reasons to believe that this was the case: the signal-to-noise (S/N) ratio was high for the selected lines and the line list we used agrees with the list compiled by Andersen & Nordstrom (1983).

For the 1994 data set, the He I lines (4026 and 4471) were studied for K_1. As the spectra are from single slit observations, these two lines were combined and cross-correlated. Thus, for this data set we used the results of the combined CCF (Fig. 1): $V_0 = -22.8$ and $K_1 = 60.2$ (km s^{-1}). However, as the resolution of the 1997 data is better than that of the 1994 data, we present the latter results for archiving purposes only (Table A1).

Because the 1997 run used an Echelle spectrograph, the selected lines were spread into different orders and were treated separately. Using the same method that we used for the 1994 data, a set of V_0 and K_1 pairs was obtained (Table 3). In Fig. 2 RV curves of the He I lines are plotted.

Table 3. Fits to CCFs of U CrB for 1997 run. The adopted value is the weighted average of all the lines.

Line	V_0	K_1	σ
He I (4026 Å)	9.2	65.2	7.9
Si II (4128 Å)	4.1	57.9	7.4
He I (4471 Å)	7.2	59.7	7.1
He I (5876 Å)	2.9	60.1	5.5
Si II (6347 Å)	9.1	56.7	6.1
Adopted	5.8	58.6	6.5

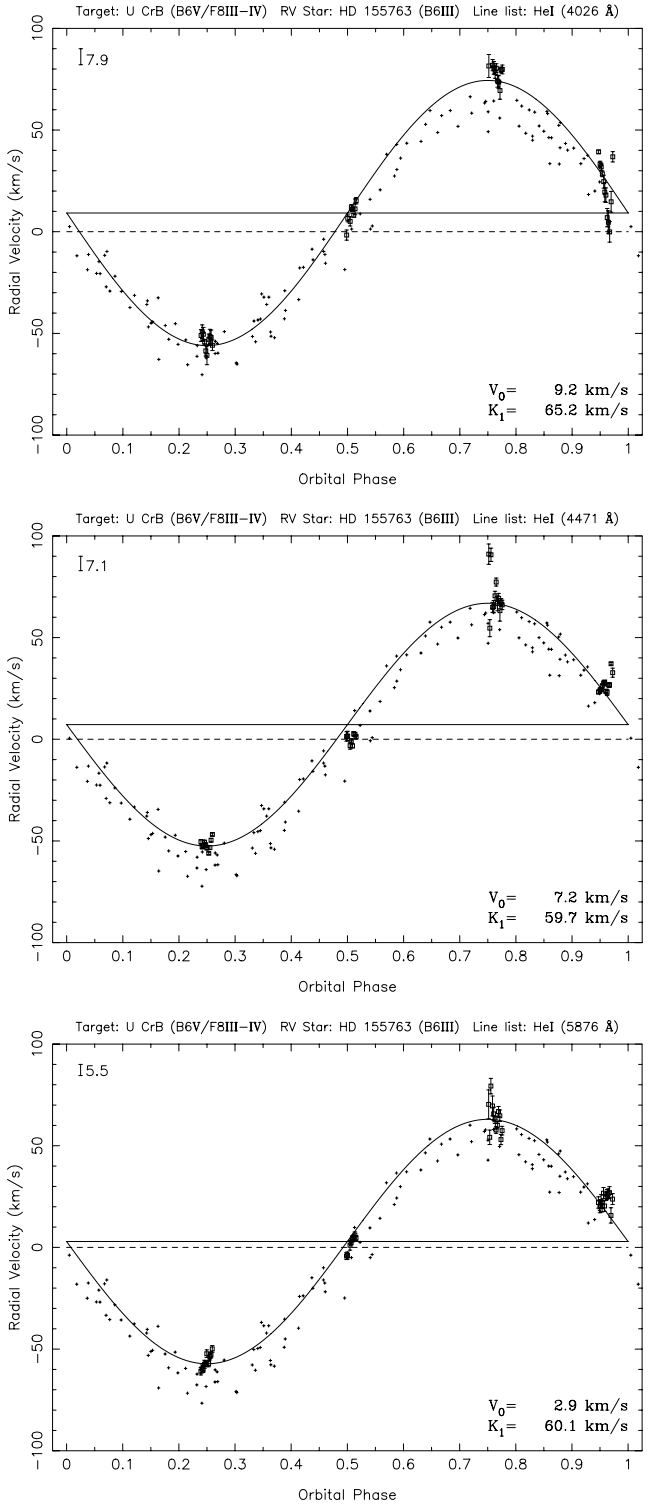

Figure 2. RV curves of He I lines (4026, 4471 and 5876 Å, from top to bottom panel, respectively) of U CrB for the 1997 run. Small plus signs represent RV values from Batten & Tomkin (1981).

The Ca I line is used to determine the value for K_2. Even though the stacked grey-scale spectra (SGSS) of the Ca I region look noisy, a fit to the CCFs gave a satisfactory RV curve which nicely fits the absorption lines on the graph (Fig. 3, right panel). The fit is shown in the left panel of Fig. 3. Phases around 0.50 and 0.95 were excluded in calculating the RV points; in the right panel of Fig. 3, it can be seen that these points have broad Ca I lines which can cause unreliable RV values. Besides, when the MAS is eclipsed by the MLS, the MAS still continues to dominate the spectrum, causing Ca I to be less prominent in the MLS spectra. The Na I(D) line was also considered for the K_2 value. However, the RV shifts of the doublet were not distinct for the MLS. Thus, for the MLS $V_0 = -14.8$ and $K_2 = 185.2$ (km s^{-1}) were adopted from the Ca I line.

4 ANALYSIS OF THE LIGHT CURVES AND PHYSICAL PARAMETERS

In this analysis, we first combined all the available data. For the photometry we used Wood (1958), van Gent (1989b), and the latest public domain *Hipparcos* observations. For the RV study, we used Batten & Tomkin (1981) (for K_1) and data from this work (for K_2).

The analysis was performed by using the Wilson–Devinney (WD) code (Wilson & Devinney 1971, revision 1992; Wilson 1992). Its 'semidetached' mode (MODE = 5) is used. In this mode, star number 2 (MLS) is assumed to be filling its Roche lobe and L_2 is coupled with the temperatures.

Because the photometric data are spread over a long time range and a small change in the period is enough to cause problems in a combined solution, phases of all the photometric data were shifted to a common system using a single period (taken from Kreiner, private communication). In Table 4, the applied phase shifts are shown. These updated light curves were then used as inputs for further WD runs. The free parameters in the run were phase shift, the luminosity of the MAS and the temperature of the MLS.

In his orbit solution, van Gent (1989a) has compared and tabulated several solutions since 1956 (his table 1). This table is reproduced in slightly modified form as Table 1. No other light-curve analysis has been performed since then. The data from Svolopoulos & Kapranidis (1972) were excluded from our analysis because of their large scatter.

The main steps of calculating the absolute orbital parameters are as follows. First, the surface temperature of the MAS ($T_{\rm eff}$) is fixed. In earlier studies Olson (1982) quoted 14 500 K for T_1 and van Gent (1989a) adopted 13 900 K from Plavec, Weiland & Dobias (1981), who obtained this value from the best fit to a Kurucz model. We ran a test on this T_1 and found exactly the same value. This was done by running the WD code with the following free parameters: phase shift, inclination, MAS Ω (surface potential) and luminosity, and the surface temperature of both components. We ran the code to obtain a grid of solutions for the primary surface temperature ranging from 12 500 to 15 500 K. When the sum of the residuals $\Sigma\ w\ (O-C)^2$ was plotted against the MAS temperature, the minimum occurred at 13 900 K. This is in very good agreement with the temperature estimation from the spectral type. After fixing this important parameter, the aim is to construct a reliable orbit with the remaining free parameters.

Although we used the K_1 value from Batten & Tomkin (1981), we preferred our own value for K_2, for a number of reasons. The first point to note is that the absolute parameters obtained by using the K_2 value from Batten & Tomkin (1981) and combining them with the photometric data would place the components in less convincing positions in the Hertzsprung–Russell (HR) diagram than the use of our K_2 (cf. Fig. 7). This is because their value of K_2 is larger than ours, implying a larger semimajor axis and hence, from Kepler's third law, larger masses. Another reason favouring our value of K_2 can be seen in Fig. 4. The data of Batten & Tomkin (1981) are sparse near quadrature and have considerable scatter, which could easily lead to a spuriously large amplitude for the fit to their data;

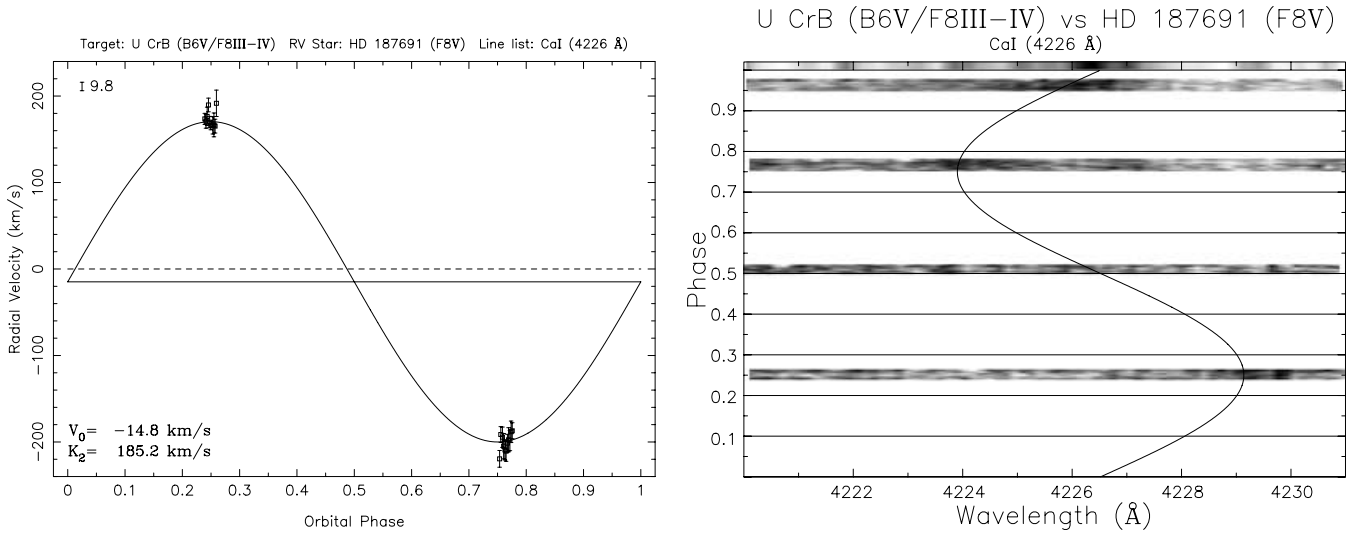

Figure 3. (Left-hand panel) RV curve of U CrB for 1997 run for the Ca I line. (Right-hand panel) SGSS of U CrB for 1997 run for the Ca I line region (see Section 2.4 for the details).

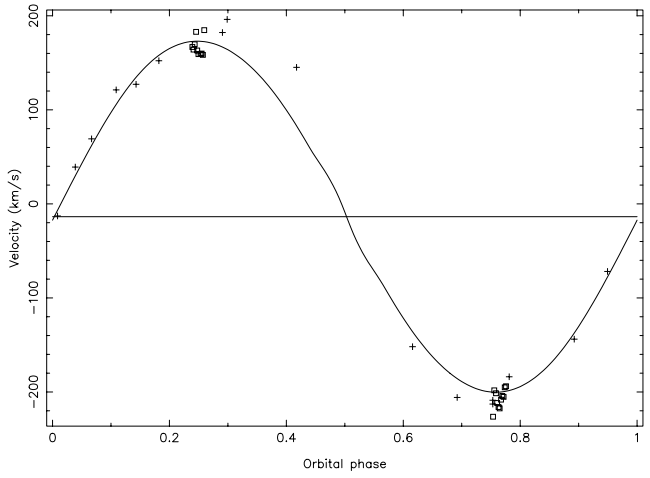

Figure 4. The velocity curves of MLS. Plus signs are from Batten & Tomkin (1981), squares are from this work and the solid line is obtained from the WD program. A common systemic velocity of -6.81 km s^{-1}, obtained from the analysis in this paper, was used to plot all three data sets.

Table 4. The phase shifts applied to each observation.

Observer	Phase shift
Wood (1958)	−0.0004
van Gent (1989b)	0.0019
Hipparcos data	0.0124

in particular, their lack of observations around phase 0.25 could fool the fitting procedure. We tried to combine the data of Batten & Tomkin (1981) with ours, and found an amplitude of 187 km s^{-1}, with rather more scatter than the value with our data alone, which tends to confirm this interpretation.

Final absolute parameters were obtained by running the WD code twice. First, to obtain the semimajor axis, the spectroscopic data were combined and the code was run with the following free parameters: semimajor axis, phase shift, systemic velocity. This determined the so-called 'spectroscopic solution' which relies only on the mass ratio obtained from spectroscopic observations (see Table 5). Thus, instead of attempting to find a photometric mass ratio, we fix the mass ratio by using the spectroscopic solution. In the second run, we applied the results from the first one and we called it 'the photometric solution'. In this run the free parameters were: phase shift, inclination, MAS Ω and luminosity, and MLS surface temperature. Finally, we computed the synthetic light curves as well as the theoretical RV curves. The stellar parameters are listed in Table 7 and they are compared with the values of van Gent (1989a) in Table 6. Velocity curves for both components are plotted in Fig. 5. Light-curve solutions for Wood (1958), van Gent (1989b), and *Hipparcos* data are plotted in Fig. 6.

Table 5. List of K_1, K_2 and q values. To calculate the adopted value, K_1 is taken from Batten & Tomkin (1981, BT) and K_2 is taken from this work. The reason for choosing K_1 from BT is that their phase coverage is much better than ours, which is a crucial point in WD calculations (see also Fig. 5).

Observer	K_1	K_2	q
BT	57.0 ± 1.0	197.0 ± 4.0	0.289 ± 0.019
This work	58.6 ± 2.0	185.2 ± 5.0	0.316 ± 0.035
Adopted			0.308 ± 0.019

5 EVOLUTIONARY CALCULATIONS: THE METHODS

5.1 The evolutionary code

In our calculations we assume that the semidetached evolution of a binary system is non-conservative, i.e. the total mass and angular momentum of a system are not conserved.

The formalism which we adopted is as follows (Muslimov & Sarna 1993; Sarna & de Greve 1994, 1996). We introduced the parameter f_1 characterizing the loss of mass from the binary system

Table 6. Absolute dimensions of U CrB, reproduced from table 1 of van Gent (1989a). The last line shows the results of this work. Numbers between brackets denote standard errors in units of the last significant decimal. Except for q, all the parameters are in solar units. The observers are: B – Batten (1956), C – Cester et al. (1977), BT – Batten & Tomkin (1981), vG – van Gent (1982), vG/ – van Gent (1989a), W – Wood (1958), SK – Svolopoulos & Kapranidis (1972), UPS – van Gent (1989b).

Observer	a	q	M_1	M_2	R_1	R_2	$\log L_1$	$\log L_2$
B	20.	0.378 (8)	6.5	2.5	3.5	5.5	2.86	2.26
C		0.38	6.7	2.6	3.5	5.3	2.85	1.33
BT	17.5	0.29	4.8	1.4	3.3	4.5	2.65	1.25
vG	17.8	0.289 (8)	4.8 (2)	1.5 (1)	3.3 (2)	4.4 (1)		
vG/W	17.8 (3)	0.299 (3)	4.86 (24)	1.45 (7)	2.83 (5)	4.93 (8)	2.43 (2)	1.20 (2)
vG/SK	17.5 (4)	0.310 (9)	4.63 (29)	1.43 (9)	2.66 (12)	4.91 (11)	2.38 (4)	1.21 (4)
vG/UPS	17.9 (3)	0.293 (5)	4.98 (25)	1.46 (8)	2.73 (7)	4.94 (9)	2.40 (3)	1.24 (2)
This work	17.6 (1)	0.308 (19)	4.74 (28)	1.46 (6)	2.79 (11)	4.83 (15)	2.41	1.20

and defined by relations

$$\dot{M} = \dot{M}_2 f_1 \quad \text{and} \quad \dot{M}_1 = -\dot{M}_2(1 - f_1), \tag{2}$$

where $\dot{M}$ is the mass-loss rate from the system, $\dot{M}_2$ is the rate of mass outflow from the secondary component and $\dot{M}_1$ is the accretion rate on to the primary component. The matter leaving the system will carry off its intrinsic angular momentum on a time-scale given by

$$\frac{\mathrm{d}\ln J}{\mathrm{d}t} = f_2 \frac{M_1 \dot{M}}{M_2(M_1 + M_2)}, \tag{3}$$

where M_1 and M_2 are the masses of the primary and secondary components, respectively. Here we have introduced the additional parameter, f_2, which describes the efficiency of the orbital angular momentum loss from the system. Note that the parameter f_2 in the equation above (unless it is equal to unity) is chosen so as to allow the period to vary as a unique function of the current masses (for given initial secondary mass M_{2i}, mass ratio $q_i = M_{2i}/M_{1i}$, and period P_i) and to be therefore independent of the variation of the mass-loss rate.

Table 7. The absolute orbit solution for U CrB. Numbers between brackets denote standard errors in units of the last significant decimal. All error estimates are probable errors. a is the semimajor axis, ϕ_δ is the phase shift, V_γ is the systemic velocity in km s^{-1} units, i is the inclination of the orbit in degrees, $T_{1(2)}$ is the surface temperature of MAS (MLS) in K, $\Omega_{1(2)}$ is the surface potential of MAS (MLS), q is the mass ratio (MAS/MLS), $L^*_{1(2)}$ is the monochromatic luminosity of MAS (MLS) for each set of observations, $F_{1(2)}$ is the ratio of the axial rotation rate to the mean orbital rate for MAS (MLS) [fixed to 1.00 (1.00)], $g_{1(2)}$ is the exponent in the gravity darkening law in terms of bolometric flux [fixed to 1.00 (0.32)], and Albedo$_{1(2)}$ is fixed to 1.00 (0.50). Light curves: W – Wood (1958), vG/UPS – van Gent (1989b).

	Photometric solution
a	17.63 (12)
ϕ_δ	0.0010 (6)
V_γ	−6.80 (4)
i	78.7 (3)
T_1	13 900.
T_2	5250. (20)
Ω_1	6.66 (31)
Ω_2	2.48
q	0.3078
$L^*_1/(L^*_1 + L^*_2)$	
W – B	0.9108 (25)
W – V	0.8497 (28)
vG/UPS – 4741	0.8920 (24)
vG/UPS – 6724	0.7853 (30)
vG/UPS – 7814	0.7339 (32)
vG/UPS – 8711	0.7041 (34)
Hipparcos – V	0.8497 (23)

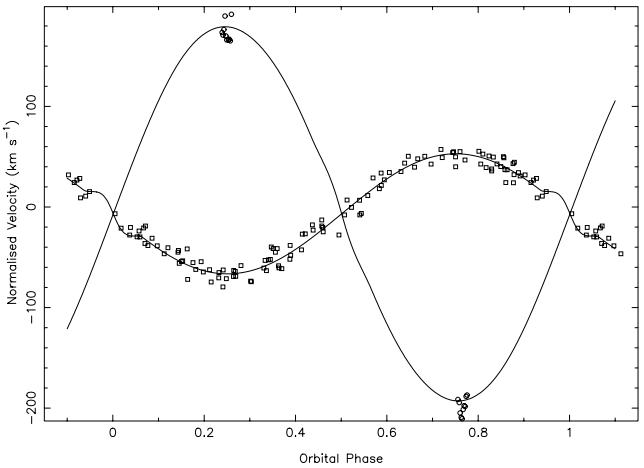

Figure 5. Velocity curves and their solutions for both components of U CrB. MAS velocity points (squares) are from Batten & Tomkin (1981) and MLS velocity points (circles) are from this work.

From the above equations and standard orbit theory we find that

$$f_2 = \frac{\Delta\log P - \Delta\log(M_1 + M_2) + 3\Delta\log(M_1 M_2)}{3[f_1 \Delta\log M_2 - \Delta\log(M_1 + M_2)]}, \tag{4}$$

where Δ represents changes in the system parameters between the observed and initial stages. Given the present orbital period and mass ratio of the system, equation (4), together with theoretical evolutionary tracks, enables us to obtain Batten & Tomkin (1981) for specified values of f_1 and f_2. The parameters f_1 and f_2 are kept constant during mass transfer. The importance of the mechanisms of mixing is discussed in more detail by Sarna (1992). We include two of them in our numerical code: the accretion effect and mixing induced by an inverted gradient of molecular weight (thermohaline mixing).

We assume also that a donor star possessing a convective envelope experiences magnetic braking, and, as a consequence of this, a system loses its orbital angular momentum. For systems with the shortest orbital periods, in the final stages of evolution, the code

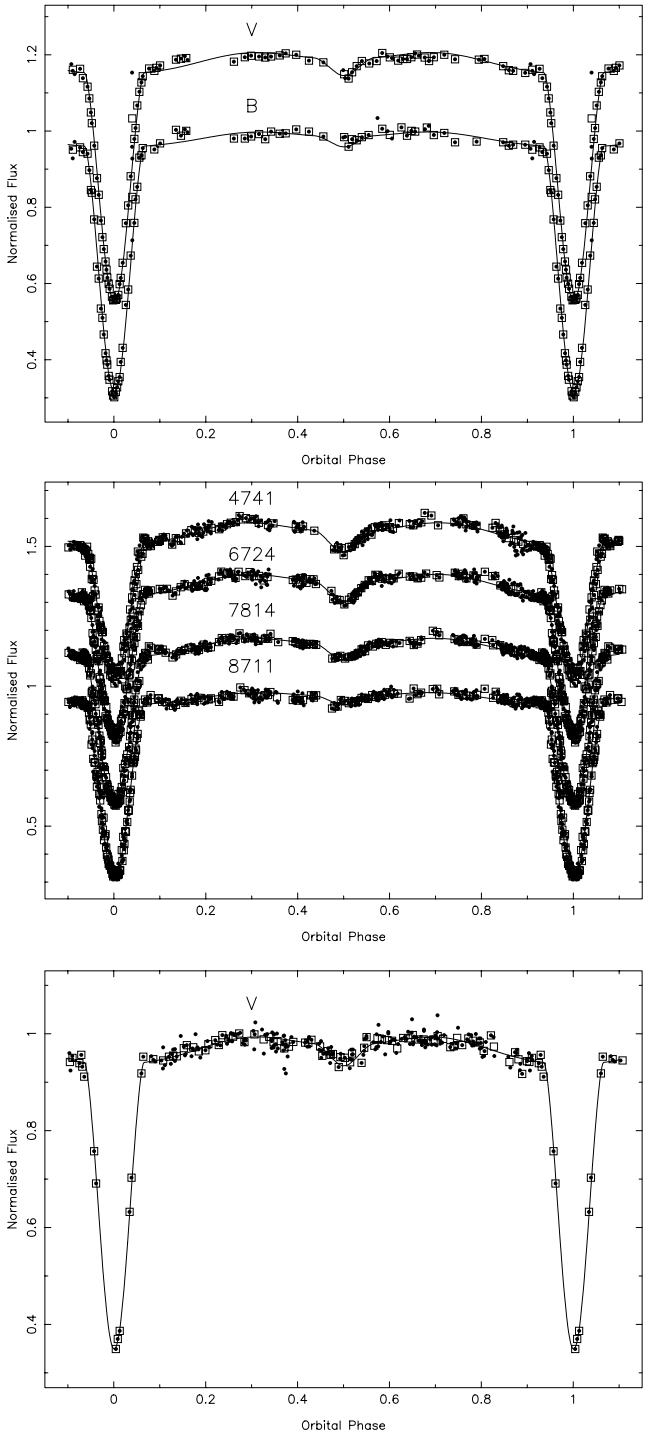

Figure 6. Light curves and their solutions for U CrB: from top to bottom panel, Wood (1958), van Gent (1989b) and *Hipparcos* data, respectively. Squares are so-called 'normal points' which are the input values for the WD program. Dots are the actual data points of the light curves.

also takes into account the loss of orbital angular momentum due to emission of gravitational radiation (Landau & Lifshitz 1971); this effect is negligible for U CrB.

The models of stars filling their Roche lobes were computed using a standard stellar evolution code based on the Henyey-type code of Paczynski (1970). Both components of the binary system were calculated simultaneously. Partial ionization of hydrogen and helium, and partial dissociation of hydrogen molecules were taken into account for the outer layer of the components. We calculated the nucleosynthesis (Fowler, Caughlan & Zimmerman 1975; Harris et al. 1983) of the elements H, He^3, He^4, C^{12}, N^{14}, O^{16} in the centre of both components. Convection was treated with the mixing-length algorithm proposed by Paczynski (1969). We solved the problem of radiative transport by employing the opacity tables of Iglesias & Rogers (1996). We used the opacity tables of Huebner et al. (1977) to fill the gaps where the tables of Iglesias & Rogers (1996) are incomplete. For temperatures less than 6000 K we used the opacities given by Alexander & Ferguson (1994) and Alexander (private communication). The contribution from conduction that is provided in the opacity tables of Huebner et al. (1977) was also included in the other tables. Population I chemical composition was assumed for the mass-losing component ($X = 0.7$; $Z = 0.03$). Finally, for elemental abundances we adopted the values of Kurucz (1979) for C, N and O: $X_{\rm C} = 0.00397$, $X_{\rm N} = 0.00143$, $X_{\rm O} = 0.00964$.

5.2 Magnetic braking

In evolutionary calculations the rate of loss of orbital angular momentum arising from magnetic braking of a donor star is usually calibrated by a parameter λ – parameter f in the notations of Verbunt & Zwaan (1981); see also Iben & Tutukov (1984) – with a value ranging from ∼0.73 (Skumanich 1972) to ∼1.78 (Smith 1979).

In this paper we calculate the evolutionary sequences making allowance for dynamo action in low-mass and Algol-type stars (Muslimov & Sarna 1996; Sarna, Muslimov & Yerli 1997). In the formula for magnetic braking, we do not use the standard λ parameter. Instead, we calculate the equipartition value of the magnetic field strength $B_{\rm eq}$ generated at the base of the stellar convection zone and then, in the formula for magnetic braking, we use the following value for the surface magnetic field strength

$$B_{\rm sur} \sim \frac{r_{\rm b} H_{\rm p}}{R_{\rm c}^2} B_{\rm eq}, \tag{5}$$

where $r_{\rm b}$ is the inner radius of the convection zone, $H_{\rm p}$ is the pressure scaleheight at the base of the convection zone, and $R_{\rm c}$ is the radius of the MLS. In our derivation of equation (5) we have assumed that the magnetic flux of the toroidal magnetic field generated at the base of the convection zone, $\Phi_{\rm tor} \sim B_{\rm eq}\ (\pi/2)\ [(r_{\rm b} + H_{\rm p})^2 - (r_{\rm b} - H_{\rm p})^2] = B_{\rm eq} 2\pi\, r_{\rm b}\, H_{\rm p}$, is equal to the magnetic flux of a large-scale poloidal field through the stellar surface, $\Phi_{\rm pol} \sim B_{\rm sur} 2\pi\, R_{\rm c}^2$.

Equation (5) implies, therefore, that the large-scale poloidal magnetic field is rather efficiently maintained by dynamo action in the MLS during its evolution as a low-mass binary. Let us write the expression for the spin angular momentum ($J_{\rm spin}$) loss from a single star due to a magnetic stellar wind in the form (see Mestel 1968; Mestel & Spruit 1987):

$$\dot{J}_{\rm spin} = -\frac{2}{3} \frac{B_{\rm sur}^2 R_{\rm c}^4 \Omega}{V_{\rm A}}, \tag{6}$$

where Ω is the angular velocity of the star and $V_{\rm A}$ is the velocity at the Alfvénic surface (where the wind speed = $V_{\rm A}$).

The surface value of the magnetic field strength given by equation (5) can then be used in the standard expression for the magnetic braking of a star (equation 6) to derive the rate of loss of orbital angular momentum from a system (assuming synchronous rotation) arising from magnetic braking

$$\left(\frac{{\rm d}\ln J}{{\rm d}t}\right)_{\rm MB} = -3 \times 10^{-7} \frac{1}{\lambda^2} \frac{m^2 r_{\rm c}^4}{m_1 a^5}\ {\rm yr}^{-1}, \tag{7}$$

where J is the orbital angular momentum of the system, m_2 and m_1 are the masses (in solar units) of the loser and the main-sequence star, respectively, $m = m_1 + m_2$, and r_c and a are the radius of the MLS and the orbital separation (both in solar units), respectively. The explicit expression for the λ parameter in equation (7) now reads

$$\lambda \sim 0.5 \frac{1}{H_{p9}^2} \frac{r_c^2}{r_{b9}} \left(\frac{m_2}{\rho_b} \right)^{1/2} T_6^{1/4} N_D^{1/2}, \quad (8)$$

where $H_{p9} \equiv H_p / 10^9$ cm, $T_6 \equiv T_{ph} / 10^6$ K, T_{ph} is the photospheric temperature of the MLS, ρ_b (g cm^{-3}) is the mass density at the base of the convection zone, $r_{b9} \equiv r_b / 10^9$ cm, and $N_D \approx (\Omega \tau_{con})^2$ is the dynamo number ($N_D = Ro^{-2}$, Ro is the so-called Rossby number).

Equation (7) shows that the efficiency of magnetic braking is rather sensitively determined by the characteristic density and pressure scaleheight of the layer in which the dynamo action is thought to occur (see Muslimov & Sarna 1996; Sarna et al. 1997). For example, in the case of the evolutionary sequence calculated for an initially main-sequence star, the efficiency of magnetic braking increases during evolution, mostly because of the increase in the density of the 'dynamo-operating' layer. In contrast, in the cases of the evolutionary sequences calculated for stars with small helium cores, the efficiency of magnetic braking, at the very late stages of evolution, substantially decreases because the dynamo-operating layer moves toward lower densities. In other words, as our calculations show (Muslimov & Sarna 1996), for the MLS evolving from a main-sequence star, the kinetic energy of convective motions near the base of the convection zone decreases during evolution but only by less than a factor of $\sim$10. By contrast, for the MLS evolving from stars with small helium cores, which are considered in this paper, the energy reservoir for the dynamo operation is reduced during evolution by a factor of $\simeq 10^3$.

6 THE EVOLUTIONARY STATUS OF U CRB

In order to further delimit the estimates of the initial parameters, we compared the set of preferred dimensions in Table 6 with the series of binary evolution by de Greve (1993). These calculations only deal with early case B mass transfer and explicitly take into account a 50 per cent mass loss from the system. We first located the mass-losing star in the mass–luminosity diagram of figures 6 and 7 in de Greve (1993). This shows that the initial mass is smaller than 5 $M_\odot$ if it is assumed to be on the increasing branch of the track. If we assume it to be on the decreasing (or horizontal) branch, then the initial mass is near 3 $M_\odot$. The position in the HR diagram puts it on the increasing branches of systems with $M_{2i} = 4$ and 5 $M_\odot$ and initial mass ratio $q_i = M_{2i}/M_{1i}$ around 1.667. However, adopting these positions results in a mass transfer rate ($\sim 10^{-7}$ $M_\odot$ yr^{-1}) that is an order of magnitude larger than the value derived by Kreiner & Ziołkowski (1978). This rules out the considered non-conservative case B, as well as a conservative case B, which results in similar period changes.

The gainer is well located on the main sequence. Because we might expect a low mass-loss rate from the small period variation, we may assume that the gainer is practically in thermal equilibrium, and hence its appearance in radius and luminosity reflects its internal stage of evolution. We therefore compare the dimensions of the gainer with a model of single stars. Using figures 3 and 4 from Sarna & de Greve (1994) which show mass–radius and mass–luminosity relations for main-sequence stars with different central hydrogen content (X_c), we locate the position of the gainer and determine its present X_c which is $X_c = 0.6 \pm 0.1$. Using this value, we can try to estimate the central hydrogen content at the onset of accretion. The star rejuvenates in the centre as a result of the increase of the convective core (de Greve & Packet 1990; Sarna 1992). Therefore, we can conclude that at the onset of mass transfer the gainer was practically on the zero-age main sequence. This indicates again that the initial mass ratio must be far from 1.

As observational constraints for our evolutionary model we have the present mass transfer rate ($\geqslant 3 \times 10^{-8}$ $M_\odot$ yr^{-1}; Kreiner & Ziołkowski 1978), the mass ratio ($q = 0.308 \pm 0.019$), the period ($P = 3.452$ d) and additionally the carbon abundance at the surface of the gainer [C/H] $= -0.41 \pm 0.20$ (Cugier 1989; Tomkin & Lambert 1994). The system initially had a mass ratio about 1.7 and evolves through a non-conservative case A with the loser close to the terminal age main sequence. The mass range of the initial primary component is restricted to 4–5 $M_\odot$.

We have investigated evolutionary models for the U CrB system using the constraints described above and the computational method discussed in Section 5.

We have chosen $M_{2,i} = 1.667\, M_{1,i}$ and P_i so that the mass transfer sets in when $X_{c2} = 0.2$. For each choice of $M_{1,i}$, the mass $M_{2,i}$ but also the values f_1 and f_2 are fixed. One of the models ($M_{2,i} = 4.5$ $M_\odot$, $q_i = 1.667$, $P_i = 1.406$ d) is presented in more detail in Figs 7 and 8.

Additionally, the chemical evolution of carbon and nitrogen on the star's surface for both components is presented in Fig. 9. We can see that the carbon abundance is inside the error-bar range, but as in the case of β Per (Sarna 1992) and U Sge (Sarna & de Greve 1994), unless the system is in an advanced phase of mass transfer, the carbon abundance is not a very sensitive factor.

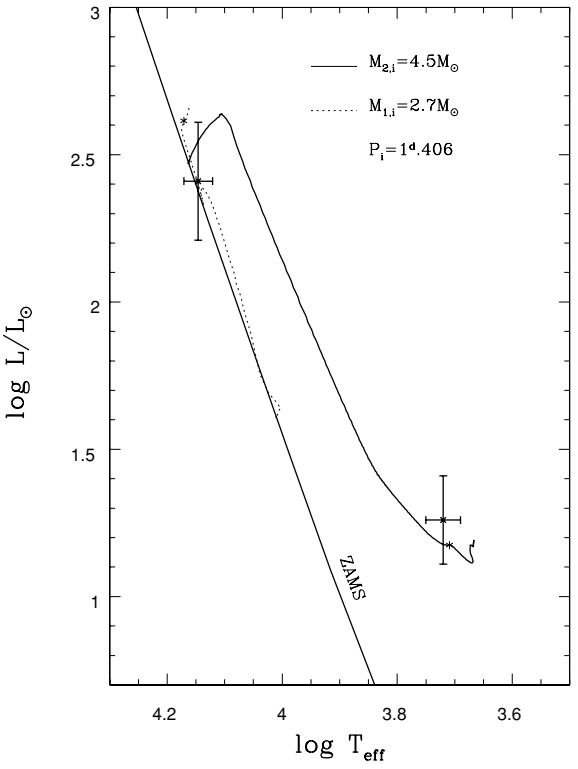

Figure 7. HR diagram of loser (solid curve) and gainer (dotted curve) of the system 4.5 $M_\odot$ + 2.7 $M_\odot$, together with the observed positions of the components of U CrB. The asterisks on the curves mark the theoretical models matching the observed mass values.

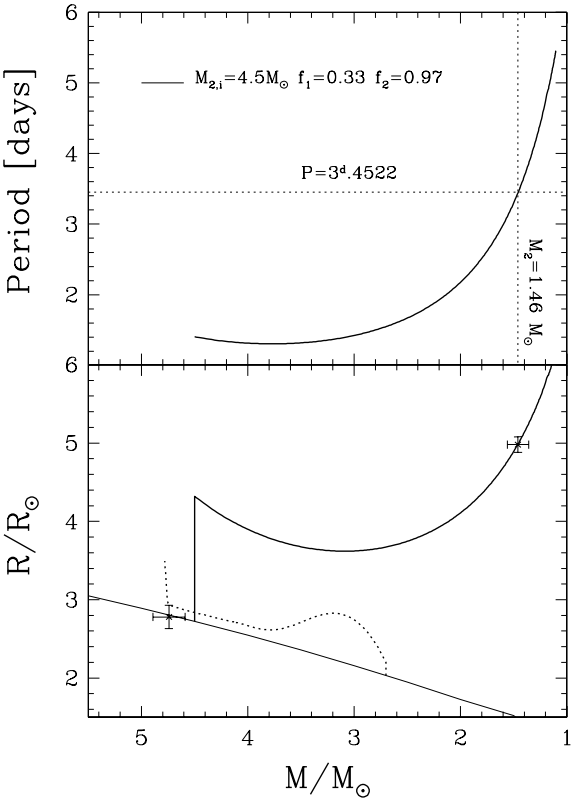

Figure 8. Period variation (upper panel) with decreasing mass of the loser for the system $4.5\,M_\odot + 2.7\,M_\odot$, for a given choice of f_1 and f_2. The dotted lines mark the values for U CrB. In the lower panel we show radius variation with mass for the two components for our system compared to the positions of the components of U CrB.

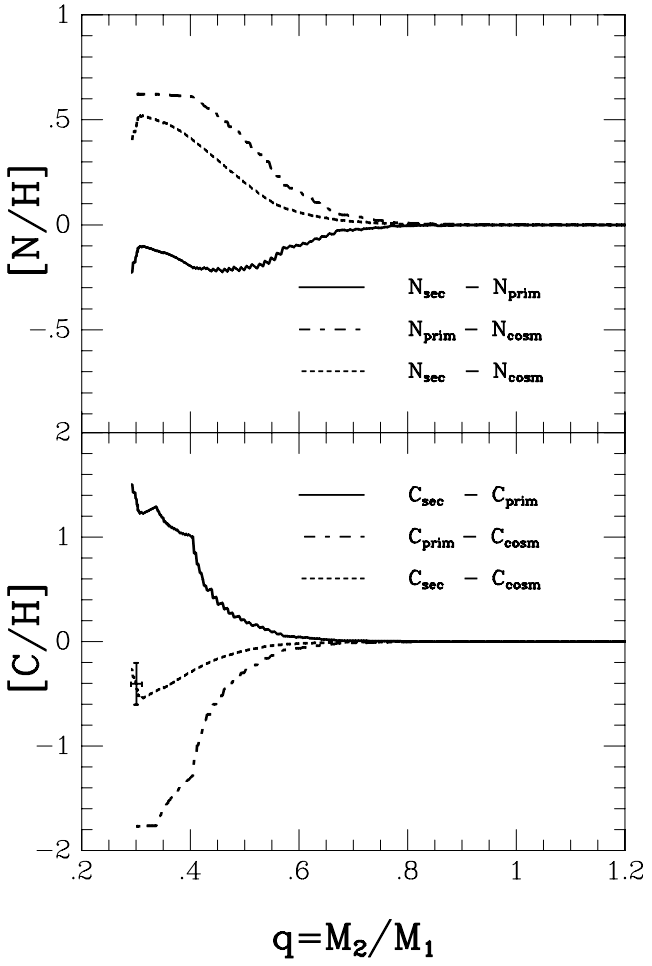

Figure 9. Variation of nitrogen (upper panel) and carbon (lower panel) with varying mass ratio.

During the semidetached evolution the fitting model loses about 14 per cent of its initial total mass and 18 per cent of the initial total orbital angular momentum. The corresponding numbers for β Per (which evolved through early case B) and U Sge (which evolved through case AB) are (15 and 30 per cent) and (6 and 2 per cent), respectively. This seems to be consistent when we remark that accretion in β Per is more rapid than that in U CrB (case A). The above result is also consistent with low values for U Sge, which is an effect of the less rapid mass transfer (initial mass ratio near unity).

We also examined a case where the secondary has initially larger mass. We chose $M_{2,i} = 5M_\odot$, resulting in the initial conditions $M_{1,i} = 3\,M_\odot$ ($q_i = 1.667$), $f_1 = 0.509$, $f_2 = 1.169$, $P_i = 1^{\rm d}.607$. Our computation shows that we cannot rule out this possibility. Almost all the computed physical parameters are inside the error range (except carbon). However, the mass flow rate is a factor of 15 higher than the value for our preferred model, $2 \times 10^{-8}\,M_\odot\ {\rm yr}^{-1}$ – which agrees with the value predicted by Kreiner & Ziołkowski (1978) $\sim 3 \times 10^{-8}\,M_\odot\ {\rm yr}^{-1}$.

The best-fitting model has the following initial conditions:

$$M_{2,i} = 4.5 \pm 0.5\,M_\odot,$$
$$M_{1,i} = 2.7 \pm 0.3\,M_\odot,$$
$$P_i = 1.4 \pm 0.2\,{\rm d},$$
$$f_1 = 0.33 \pm 0.15,$$
$$f_2 = 1.0 \pm 0.2.$$

The errors provide an estimate of the effect of the observational errors and of our free parameter f_2.

7 MAGNETIC ACTIVITY AND EVOLUTION OF U CRB

We have calculated an evolutionary sequence that fits the present parameters of U CrB. The initial parameters are presented in the previous section.

Fig. 10 displays the evolution of the thickness of the convective zone for the secondary component of U CrB. It shows that a relatively thick convective envelope has developed by the end of the active phase of mass transfer. The situation is different for the two other systems that we analysed (Sarna, Yerli & Muslimov 1998): β Per and U Sge. They show thick convective envelopes at the very beginning of the semidetached phase (see figure 1 of Sarna et al. 1998). This difference can be explained by the fact that the initial mass of the secondary in U CrB is much higher than in β Per ($M_{2,i} = 2.81\ M_\odot$) or in U Sge ($M_{2,i} = 3.27\ M_\odot$). β Per is in the final stage of building up its thick convective zone, while U CrB and U Sge are just at the beginning of forming such a zone.

The results of our calculations for the standard $\alpha - \omega$ dynamo are summarized in Fig. 11. The upper panel of Fig. 11 shows that the parameter λ changes substantially during the evolution of the

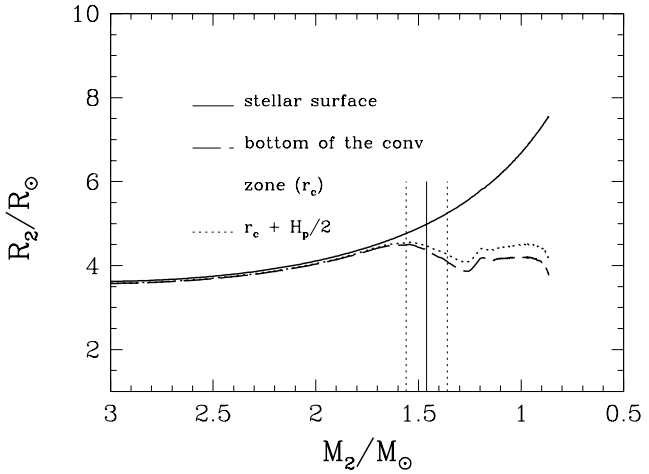

Figure 10. Thickness of the convective zone as a function of the mass of a donor star, calculated for the evolving stellar model of a donor star in U CrB. The evolutionary calculations are performed for the following initial parameters of U CrB: $M_{2,i} = 4.5$ M$_\odot$, $q = M_{2,i}/M_{1,i} = 1.667$, $P_i = 1.4$ d, $f_1 = 0.33$ and $f_2 = 0.97$. The position of the donor for U CrB is marked by the thin vertical solid line. The errors in mass determination are marked by dashed vertical lines.

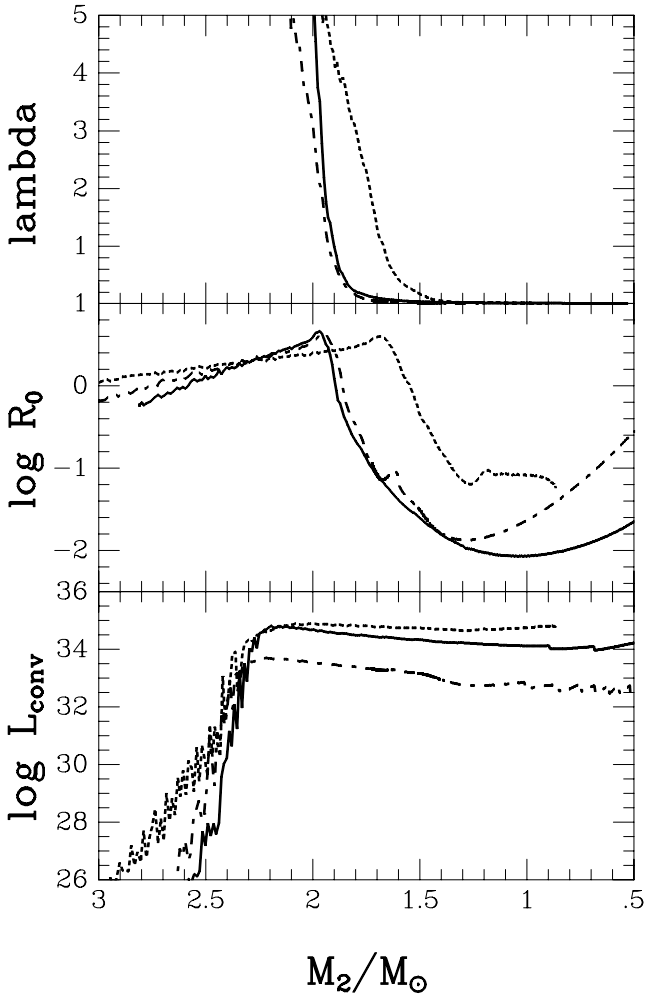

Figure 11. Results of dynamo calculations for U CrB (dotted line), β Per (solid line) and U Sge (dash-dotted line) are shown in each panel. The upper panel shows the value of the parameter λ as a function of the mass of the donor star. The middle panel shows the value of the Rossby number as a function of the mass of the donor star. The lower panel shows the convective luminosity at the outermost boundary of the convective zone as a function of the mass of the donor star.

mass-losing star in the binary. As is seen from the figure, the efficiency of magnetic braking is high only during a certain phase of semidetached evolution – while the mass of the donor star decreases from 1.5 to 0.3–0.2 M$_\odot$. In the middle panel of Fig. 11 we demonstrate the evolution of the Rossby number. In the present evolutionary stage of U CrB, the Rossby number is small (comparable to U Sge) but one range of magnitude higher than the minimum level. This phase can be associated with the beginning of enhanced magnetic activity (dynamo action) in the donor star. In the lower panel of Fig. 11 we present the evolution of the convective luminosity (calculated at the upper boundary of the convective zone) for a star: U CrB (dotted line), β Per (solid line) and U Sge (dash-dotted line). The result for U CrB is consistent with our earlier calculations (Sarna et al. 1998). The convective luminosity for U CrB is higher than for β Per and U Sge and therefore the X-ray luminosity is higher as well (see table 1 of Sarna et al. 1998).

8 CONCLUSIONS

The results of our investigations can be summarized as follows.

(i) A new set of RV semi-amplitudes has been found: $K_1 = 58.6 \pm 2.0$ km s^{-1}, $K_2 = 185.2 \pm 5.0$ km s^{-1}.

(ii) Combining earlier photometric data (Wood 1958; van Gent 1989b) and the data set from the *Hipparcos* public archive with the present spectroscopic work, a new set of absolute parameters was calculated using the WD program. The system parameters are as follows: $M_1 = 4.74 \pm 0.28$ M$_\odot$, $M_2 = 1.46 \pm 0.06$ M$_\odot$, $R_1 = 2.79 \pm 0.11$ R$_\odot$, $R_2 = 4.83 \pm 0.15$ R$_\odot$, $\log L_1/L_\odot = 2.41$, $\log L_2/L_\odot = 1.20$.

(iii) This new orbit gives a slightly smaller $q = 0.308 \pm 0.019$ value.

(iv) We used orbital and physical parameters described in Section 4 to calculate the evolutionary status of U CrB. We discuss the system from a non-conservative point of view, concerning mass transfer, and considering mass and angular momentum losses from the system. The non-conservative evolution has given reasonably good agreement with observational parameters. From computations, we have determined the initial period and the mass ratio to be around 1.4 d and 1.667, respectively. During its evolution, the system has lost about 14 per cent of its initial total mass ($\sim$1 M$_\odot$) and around 18 per cent of its initial total angular momentum. However, due to uncertainties in the orbital and physical data for U CrB, the determination of initial parameters can be affected by an error as large as 20 per cent.

(v) We examined the possibility of probing dynamo action in the mass-losing star of U CrB. We showed that the mass-losing component is at the beginning of a very active magnetic phase of evolution. We also showed that the convective luminosity, calculated at the upper boundary of the convective zone, explains the high X-ray flux from this system very well.

ACKNOWLEDGMENTS

This work was supported in part by the Polish State Committee for Scientific Research under grant 2-P03D-001.10 and 2-P03D-005-16. This work was funded in part by the studentship of ODTÜ

(Middle East Technical University, Ankara, Turkey) and YÖK (Higher Education Council of Turkey) which was awarded to SKY. SKY also thanks P.F.L. Maxted for his valuable help in the RV curve-fitting routine. The data reduction was carried out on the Sussex Starlink node.

REFERENCES

Albright G. E., Richards M. T., 1996, ApJ, 459, L99
Alexander D. R., Ferguson J. W., 1994, ApJ, 437, 879
Andersen J., Nordstrom B., 1983, A&A, 122, 23
Bakos G. A., Tremko J., 1981, J. R. Astron. Soc. Can., 75, 124
Batten A. H., 1956, MNRAS, 116, 552
Batten A. H., Tomkin J., 1981, Publ. Dom. Astrophys. Obs., 15, 419
Catalano S., Cristaldi S., Lacona G., 1966, Mem. Soc. Astron. It., 37, 213
Cester B., Fedel B., Giuricin G., Mardirossian F., Pucillo M., 1977, A&A, 61, 469
Cugier H., 1989, A&A, 214, 168
de Greve J. P., 1993, A&AS, 97, 527
de Greve J. P., Packet W., 1990, A&A, 230, 97
Etzel P. B., Olson E. C., Senay M. C., 1995, AJ, 109, 1269
Fowler W. A., Caughlan G. R., Zimmerman B. A., 1975, ARA&A, 13, 69
Hamuy M., Walker A. R., Suntzeff N. B., Gigoux P., Heathcote S. R., Phillips M. M., 1992, PASP, 104, 533
Harris M. J., Fowler W. A., Caughlan G. R., Zimmerman B. A., 1983, ARA&A, 21, 165
Heintze J. R. W., van Gent R. H., 1989, Space Sci. Rev., 50, 257
Hill G., 1993, in Leung K. C., Nha I.-S., eds, ASP Conf. Ser. Vol. 38, New Frontiers in Binary Star Research. Astron. Soc. Pac., San Francisco, p. 127
Horne K., 1986, PASP, 98, 609
Huebner W. F., Merts A. L., Magee N. H. J., Argo M. F., 1977, Technical Report LA–6760–M, Astrophysics Opacity Library. Los Alamos Scientific Lab
Iben I., Tutukov A. V., 1984, ApJ, 284, 719
IDL, 1997, Technical report, Reference Guide. Research Systems Inc.
Iglesias C. A., Rogers F. J., 1996, ApJ, 464, 943
Kondo Y., McCluskey G. E., Wu C.-C., 1981, ApJS, 47, 333
Kordylewski B., Szafraniec R., 1957, Acta Astron., 7, 177
Kreiner J. M., Ziołkowski J., 1978, Acta Astron., 28, 497
Kurucz R. L., 1979, ApJS, 40, 1
Landau L. D., Lifshitz E. M., 1971, Course of Theoretical Physics 3rd Rev. Engl. edition. Pergamon Press, Oxford
Mestel L., 1968, MNRAS, 138, 359
Mestel L., Spruit H. C., 1987, MNRAS, 226, 57
Muslimov A. G., Sarna M. J., 1993, MNRAS, 262, 164
Muslimov A. G., Sarna M. J., 1996, ApJ, 464, 867
Oke J. B., Gunn J. E., 1983, ApJ, 266, 713
Olson E. C., 1980, ApJ, 237, 496
Olson E. C., 1982, ApJ, 257, 198
Olson E. C., 1984, PASP, 96, 376
Paczynski B., 1969, Acta Astron., 19, 1
Paczynski B., 1970, Acta Astron., 20, 47
Pearce J. A., 1935, Publ. Am. Astron. Soc., 8, 219
Plaskett J. S., 1920, Publ. Dom. Astrophys. Obs., 1, 187
Plavec M. J., Weiland J. L., Dobias J. J., 1981, BAAS, 13, 803
Richards M. T., Albright G. E., Bowles L. M., 1995, ApJ, 438, L103
Sarna M. J., 1992, MNRAS, 259, 17
Sarna M. J., de Greve J.-P., 1994, A&A, 281, 433
Sarna M. J., de Greve J.-P., 1996, QJRAS, 37, 11
Sarna M. J., Muslimov A., Yerli S. K., 1997, MNRAS, 286, 209
Sarna M. J., Yerli S. K., Muslimov A. G., 1998, MNRAS, 297, 760
Skumanich A., 1972, ApJ, 171, 565
Smith M. A., 1979, PASP, 91, 737
Svolopoulos S. N., Kapranidis S., 1972, Inf. Bull. Var. Stars, 731, 1
Tomkin J., Lambert D. L., 1994, PASP, 106, 365
van Gent R. H., 1982, Inf. Bull. Var. Stars, 2140, 1
van Gent R. H., 1989a, Space Sci. Rev., 50, 264
van Gent R. H., 1989b, A&AS, 77, 471
Verbunt F., Zwaan C., 1981, A&A, 100, L7
Wilson R. E., 1992, Documentation of Eclipsing Binary Computer Model. University of Florida, Florida
Wilson R. E., Devinney E. J., 1971, ApJ, 166, 605
Wood D. B., 1958, ApJ, 127, 351

APPENDIX A: RV VALUES

We present the measurements of RV values for both 1994 and 1997 data sets. In all three tables, we give the heliocentric Julian date, phase and RV (in km s^{-1}).

Table A1. HJD versus RV for two He I (4026 and 4471 Å) lines of the 1994 data set (K_1 value).

HJD[a]	Phase	RV_{pri}	HJD[a]	Phase	RV_{pri}
49430.7258	0.2012	−81.14	49432.6079	0.7464	38.60
49430.7386	0.2049	−81.05	49432.6202	0.7499	36.77
49430.7509	0.2085	−78.32	49432.6365	0.7547	37.37
49430.7632	0.2120	−70.15	49432.6488	0.7582	41.22
49431.5420	0.4376	−61.30	49432.6611	0.7618	48.37
49431.5543	0.4412	−64.45	49432.6769	0.7664	40.69
49431.5666	0.4448	−64.52	49432.6892	0.7699	38.10
49431.5819	0.4492	−60.63	49432.7015	0.7735	42.63
49431.5942	0.4527	−57.18	49432.7169	0.7780	36.04
49431.6065	0.4563	−47.72	49432.7292	0.7815	47.53
49431.6218	0.4607	−56.91	49432.7415	0.7851	41.73
49431.6341	0.4643	−47.67	49432.7540	0.7887	43.49
49431.6464	0.4679	−51.76	49434.6867	0.3485	−52.67
49431.6621	0.4724	−33.74	49434.7015	0.3528	−65.26
49431.6744	0.4760	−34.05	49434.7138	0.3564	−65.08
49431.6867	0.4796	−30.48	49434.7261	0.3600	−67.52
49431.7084	0.4858	−28.79	49434.7412	0.3643	−57.69
49431.7207	0.4894	−30.96	49434.7535	0.3679	−63.65
49431.7330	0.4929	−36.03	49434.7658	0.3714	−63.01
49431.7480	0.4973	−31.70	49435.7035	0.6431	27.68
49431.7603	0.5009	−37.53	49435.7158	0.6467	18.70
49432.5561	0.7314	24.72	49435.7281	0.6502	26.55
49432.5684	0.7350	30.56	49435.7429	0.6545	21.60
49432.5807	0.7385	30.64	49435.7552	0.6581	24.06
49432.5956	0.7428	38.10	49435.7675	0.6616	12.76

Note: [a]HJD ≡ HJD − 2 400 000.

Table A2. HJD versus RV for the Ca I (4226 Å) line of the 1997 data (K_2 value).

HJD[a]	Phase	RV_{sec}	HJD[a]	Phase	RV_{sec}
50583.9055	0.2391	173.61	50585.6893	0.7558	−191.39
50583.9129	0.2412	170.85	50585.6991	0.7586	−194.52
50583.9202	0.2433	176.50	50585.7064	0.7607	−204.87
50583.9278	0.2455	189.73	50585.7137	0.7628	−209.22
50583.9351	0.2476	169.93	50585.7212	0.7650	−210.63
50583.9424	0.2497	166.03	50585.7285	0.7671	−201.35
50583.9535	0.2530	166.17	50585.7359	0.7692	−197.47
50583.9608	0.2551	166.67	50585.7436	0.7715	−198.35
50583.9682	0.2572	165.26	50585.7510	0.7736	−188.22
50583.9761	0.2595	191.60	50585.7583	0.7757	−187.06
50585.6820	0.7536	−219.50			

Note: [a]HJD ≡ HJD − 2 400 000.

Table A3. HJD versus RV for three He I (4026, 4471, 5876) and two Si II (4128, 6347) lines of the 1997 data set (K_1 value).

HJD[a]	Phase	He I 4026	Si II 4128	He I 4471	He I 5876	Si II 6347
50582.8977	0.9471	39.29	27.99	23.24	22.11	30.09
50582.9066	0.9497	33.18	28.33	23.95	19.98	33.85
50582.9139	0.9518	31.95	29.80	24.60	22.55	29.10
50582.9212	0.9539	28.44	29.74	26.22	20.17	27.06
50582.9287	0.9561	24.64	26.95	27.50	26.70	31.67
50582.9360	0.9582	19.47	29.12	28.18	20.35	30.77
50582.9433	0.9603	17.99	30.60	23.58	24.98	30.40
50582.9510	0.9626	6.93	25.41	23.05	25.96	40.69
50582.9583	0.9647	4.66	26.55	26.84	26.50	
50582.9656	0.9668	−0.08	27.34	26.65	26.95	
50582.9752	0.9696	14.72	33.55	37.16	15.74	27.31
50582.9853	0.9725	36.84	38.52	32.76	23.78	
50583.9055	0.2391	−51.03	−52.00	−50.44	−60.89	−46.98
50583.9129	0.2412	−49.13	−54.12	−52.79	−59.68	−48.08
50583.9202	0.2433	−50.42	−51.92	−52.44	−59.96	−52.49
50583.9278	0.2455	−54.17	−55.97	−50.81	−57.46	−42.95
50583.9351	0.2476	−58.59	−55.64	−51.99	−57.22	−44.54
50583.9424	0.2497	−60.79	−54.04	−53.38	−52.27	−46.42
50583.9535	0.2530	−52.89	−55.63	−56.07	−57.09	−47.59
50583.9608	0.2551	−51.54	−53.81	−53.21	−53.65	−48.26
50583.9682	0.2572	−52.01	−52.81	−49.64	−52.87	−48.28
50583.9761	0.2595	−55.83	−54.35	−46.80	−49.92	−47.44
50584.8009	0.4984	−1.65	2.85	1.38	−4.23	−0.23
50584.8082	0.5005	6.57	−0.37	1.66	−3.98	0.11
50584.8230	0.5048	5.09	2.92	−3.15	1.05	8.64
50584.8303	0.5069	11.84	7.41	−0.88	2.40	5.76
50584.8377	0.5091	10.98	7.42	−3.26	4.24	2.92
50584.8452	0.5112	8.07	3.50	2.69	4.86	4.70
50584.8525	0.5134	11.23	2.28	2.31	6.05	6.25
50584.8598	0.5155	15.23	3.66	1.19	4.63	7.26
50585.6746	0.7515	81.51			70.36	65.68
50585.6820	0.7536		61.93	54.62	54.15	64.65
50585.6893	0.7558		60.28		79.34	
50585.6991	0.7586	81.90		64.88	69.54	
50585.7064	0.7607	80.62		65.22	65.70	88.56
50585.7137	0.7628	78.23	61.27	70.56	62.80	64.69
50585.7212	0.7650	80.45	59.85	77.31	57.76	60.55
50585.7285	0.7671	74.04	58.97	66.78	60.03	66.43
50585.7359	0.7692	73.61	51.12	69.36	66.81	68.11
50585.7436	0.7715	69.43	57.82	63.24	64.75	71.76
50585.7510	0.7736	79.59	63.05	67.40	53.05	59.48
50585.7583	0.7757	79.80	63.11	66.10	57.44	57.92

Note: [a]HJD ≡ HJD − 2 400 000.

This paper has been typeset from a TEX/LATEX file prepared by the author.